Sinopfbd, 2024; 10(1): 165-187 **https://doi.org/10.33484/sinopfbd.1664284**

Sinop Üniversitesi Fen Bilimleri Dergisi
Sinop Uni J Nat Sci
E-ISSN: 2564-7873

https://dergipark.org.tr/tr/pub/sinopfbd

A Study on the Synthesis, Crystallographic Structure, DFT Calculations, Hirshfeld Surface Analysis, Drug-likeness and Molecular Docking of the Julolidene-Based Schiff Base Containing Compound

Seher MERAL[1] Cem Cüneyt ERSANLI[2] Zeynep KELEŞOĞLU[2] and Ayşen ALAMAN AĞAR[3]

How to cite: Meral, S., Ersanli, C. C., Kelesoglu, Z., & Agar Alaman, A. (2025). A study on the synthesis, crystallographic structure, DFT calculations, Hirshfeld surface analysis, drug-likeness and molecular docking of the julolidene-based Schiff base containing compound. *Sinop Üniversitesi Fen Bilimleri Dergisi, 10*(1), 165-187. https://doi.org/10.33484/sinopfbd.1664284

Research Article

Corresponding Author
Cem Cüneyt ERSANLI
ccersanli@sinop.edu.tr

ORCID of the Authors
S.M: 0000-0002-6309-8936
C.C.E: 0000-0002-8113-5091
Z.K: 0000-0001-9538-9140
A.A.A: 0000-0002-1316-4835

Received: 24.03.2025
Accepted: 13.06.2025

Abstract

This study gives an in-depth investigation of the molecular structure of a julolidene-based molecule, **(**$C_{36}H_{50}N_4O_2$**)**. The investigation comprises the X-ray diffraction, density functional theory calculations, Hirshfeld surface analysis, drug similarity evaluation, and molecular docking simulations**.** The compound's structure was initially derived from X-ray coordinates and then optimized using the B3LYP density functional theory method with the 6-31G(d,p) and 6-311G(d,p) basis sets. In the present paper, the detailed molecular interactions and X-ray crystal structure of this molecule are discussed. The space group is $P\bar{1}$ and has the following unit cell parameters: a = 6.8512 (9) Å, b = 9.9748 (14) Å, c = 13.892(3) Å, α = 74.679 (13)º, β = 86.608 (13)º, γ = 75.049 (11)º, V = 884.6 (2) Å^3, Z = 1. The julolidene-based compound is crystallized with only half of the molecule in the asymmetric unit, which has reverse symmetry. A complex network comprised of O–H···N and C–H···O hydrogen bonds, and C–H···π interactions stabilizes the crystal structure, forming supramolecular architectures. The synthesized compound's theoretical parameters were compared with experimental findings. The optimized structure was analyzed at the same theoretical level, encompassing frontier molecular orbital analysis, molecular electrostatic potential, and chemical reactivity indices. Hirshfeld surface assessment was employed to anticipate molecular interactions. In addition, a drug similarity study was performed on the synthesized compound. Finally, an analysis of molecular docking for the compound under investigation was conducted.

Keywords: Julolidene, X-ray, DFT studies, drug-likeness, Hirshfeld surface analysis, molecular docking analysis

Juloliden Bazlı Schiff Bazı İçeren Bileşiğin Sentezi, Kristalografik Yapısı, DFT Hesaplamaları, Hirshfeld Yüzey Analizi, İlaç Benzerliği ve Moleküler Yerleştirme Üzerine Bir Çalışma

[1]Sinop University, Boyabat Vocational School, Department of Property Protection and Security, Sinop, Turkey

Öz

Bu çalışma, juloliden bazlı bir molekülün ($C_{36}H_{50}N_4O_2$) moleküler yapısının derinlemesine bir incelemesini sunmaktadır. Araştırma X-ışını kırınımı, yoğunluk fonksiyonel teorisi hesaplamaları, Hirshfeld yüzey analizi, ilaç benzerliği değerlendirmesi ve moleküler yerleştirme

[2]Sinop University, Faculty of Arts and Sciences, Department of Physics, Sinop, Turkey

[3]Ondokuz Mayıs University, Faculty of Sciences, Department of Chemistry, Samsun, Turkey

simülasyonlarını içermektedir. Bileşiğin yapısı ilk olarak X-ışını koordinatlarından türetilmiş ve daha sonra 6-31G(d,p) ve 6-311G(d,p) temel setleri ile B3LYP yoğunluk fonksiyonel teorisi yöntemi kullanılarak optimize edilmiştir. Bu makalede, bu molekülün ayrıntılı moleküler etkileşimleri ve X-ışını kristal yapısı tartışılmaktadır. Uzay grubu $P\bar{1}$ ve aşağıdaki birim hücre parametrelerine sahiptir: a = 6.8512 (9) Å, b = 9.9748 (14) Å, c = 13.892(3) Å, α = 74.679 (13)º, β = 86.608 (13)º, γ = 75.049 (11)º, V = 884.6 (2) Å^3, Z = 1. Juloliden bazlı bileşik, ters simetriye sahip asimetrik birimdeki molekülün sadece yarısı ile kristalize edilmiştir. O–H···N ve C–H···O hidrojen bağları ve C–H···π etkileşimlerinden oluşan karmaşık bir ağ, kristal yapıyı stabilize ederek supramoleküler mimariler oluşturur. Sentezlenen bileşiğin teorik parametreleri deneysel bulgularla karşılaştırılmıştır. Optimize edilmiş yapı, sınır moleküler orbital analizi, moleküler elektrostatik potansiyel ve kimyasal reaktivite indekslerini kapsayan aynı teorik düzeyde analiz edilmiştir. Moleküler etkileşimleri tahmin etmek için Hirshfeld yüzey değerlendirmesi kullanılmıştır. Buna ek olarak, ilaç benzerliği çalışması şema üzerinde gerçekleştirilmiştir.

Anahtar Kelimeler: Juloliden, X-ışını, DFT çalışmaları, ilaç-benzerliği, Hirshfeld yüzey analizi, moleküler kenetlenme analizi

Introduction

Julolidene is a group of chemically active and stable molecules containing a reactive nitrogen atom in a polycyclic system [1]. This heteroaromatic compound features an electron-donating group and an electron-accepting group linked by a π-conjugated framework, utilized in fluorescent turn-on sensors. Derivatives of julolidene enable efficient measurement of microenvironmental changes in solvent media, providing interesting information, especially in biological or monitoring applications [2, 3]. Conjugated electron systems can be examined based on the changes observed in the photophysical properties of the julolidene molecule after interacting with the target molecule and these changes also bring innovations to important fluorescent applications such as determining ions, biological imaging, and energy conversions [4-7]. In this context, designing synthesis methods that allow for easy and high-yield addition of more conjugation and electron-withdrawing or -donating functional groups to the main molecule may allow for determining many highly sensitive molecules [8]. Conversion of carbonyl to imine group is a synthesis route that can be used to add C=N and also different functional groups to the parent molecule with high yield. It can be realized under moderate conditions and it is known that the double bond structure of the imine group in particular increases the electron density and conjugation of this compound, resulting in an increased photochemical reactivity. These double-bond systems facilitate the molecule to become excited with light energy and subsequently form reactive molecules [9]. Julolidene which attracts attention with its electro-optic properties, especially the Schiff Base derivatives, has been studied regarding their biological properties. It has been stated that their passage through the cell membrane is remarkable with their dominant lipophilic character [10, 11]. These molecule groups to which electron-donating or -withdrawing groups are attached can form coordination compounds with metal ions and are particularly involved in catalytic activity applications. It is

considered as an important development in the studies stating that Schiff Bases obtained from julolidene compounds can be used as important fluorescence detectors, especially for analyzing metal ions [12].

The photophysics of Schiff bases derived from julolidene have been studied widely due to their unique electronic and structural characteristics, which enabled drastic advancement in the fields of fluorescence sensing, biological imaging, and catalysis. Their wonderful properties are still stimulating the synthesis of new derivatives bearing particular functionalities. In particular, replacement of the julolidene skeleton with enhanced metal-binding capability and biological affinity remains an area of research under progress. Despite such developments, there are no prior reports on the rational design, high-yield synthesis, and exhaustive structural characterization -experimental and theoretical- of a symmetrical julolidene Schiff base with a tethered alkyl linker for enhancing lipophilicity and membrane permeability. In the present work, this fundamental gap is addressed by the synthesis of a new julolidene derivative that is structurally new and functionally improved for possible biological application. In this work, we report the synthesis of a novel molecule, 9,9'-((1*E*,1'*E*)-(ethane-1,2-diylbis(azanylylidene))bis(methanylylidene))bis(1,1,7,7-tetramethyl-1,2,3,5,6,7-hexahydropyrido[3,2,1-ij]quinolin-8-ol) (EAMTPQ), with a symmetrical, tetra-dentate, cage-type structure that is appropriate for metal ion coordination and a terminal alkyl chain for enhanced lipophilicity. The structural and functional characteristics were unveiled by single-crystal X-ray diffraction, density functional theory (DFT) calculations, and molecular docking against the BRAF V600E oncogenic target. This crystallographic-computational analysis hereby discloses the first complete picture of such a lipophilic julolidene Schiff base and establishes a foundation for its prospective use in biologically relevant systems. The primary objective was to elucidate the structural properties of the synthesized compound using experimental techniques, particularly X-ray diffraction analysis. The research includes the synthesis of the desired compound, structural determination via X-ray crystallography, and computational studies utilizing DFT. The molecular structure derived from X-ray diffraction was subsequently refined using the DFT-B3LYP approach, applying the 6-31G(d,p) and 6-311G(d,p) basis sets. The geometric parameters determined experimentally and their counterparts computationally predicted were compared through a comparative analysis. Additionally, a molecular potential map was constructed using the same computational framework, and frontier molecular orbitals (FMOs) were analyzed, with a particular focus on spin transitions. A molecular electrostatic potential (MEP) analysis was conducted to explore the electronic properties and intermolecular interactions further. The crystal structure was studied for intermolecular interactions using Hirshfeld surface (HS) analysis and fingerprint plot generation. Furthermore, a molecular docking (MD) study was performed to assess the binding interactions of the EAMTPQ molecule with the BRAF V600E mutant protein (PDB ID: 5CSW) [13]. The docking simulations were executed using AutoDock Vina 1.5.6 [14], and the binding interactions were visualized through Biovia Discovery Studio software, allowing for a detailed interpretation of molecular binding affinities [15].

Experimental and Theoretical Details

Synthesis of the EAMTPQ

The EAMTPQ was obtained according to [16] (Figure 1). The synthesized symmetric Schiff Base was crystallized using a mixture of ethanol and methanol.

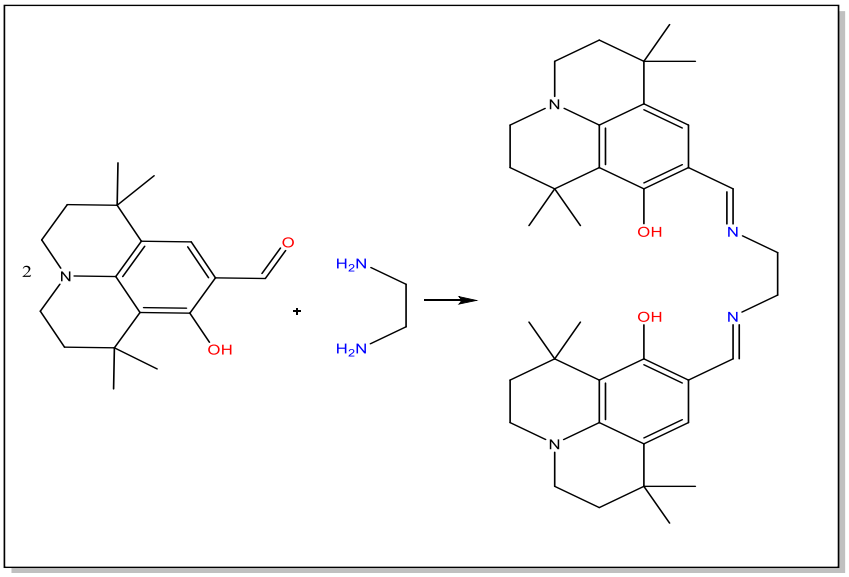

Figure 1. *Methodology for the preparation of EAMTPQ [16]*

Crystallographic Methods

The crystallographic analysis of EAMTPQ was conducted using a STOE IPDS II CCD X-ray diffractometer with graphite-monochromatized Mo-Kα radiation. Data acquisition was conducted at 293(2) K. X-AREA and X-RED32 software [17] were utilized for the data acquisition, cell refinement, data reduction, and analysis. The crystal structure solution employed direct methods with the SHELXT program [18], and the refinement was carried out using a full-matrix least-squares technique with SHELXL2018/3 [19]. WinGX [20] software was utilized for preparing publication materials, while ORTEP-III [21] and Mercury [22] were used for the graphical representation of the single-crystal X-ray data. Anisotropic thermal parameters were given to atoms that do not contain hydrogen. The positional parameters of all hydrogen atoms bonded to carbon atoms were determined geometrically and set to ride on their respective carbon atoms, with C-H distances of 0.93 Å (aromatic), 0.98 Å (CH), 0.97 Å (CH_2), and 0.96 Å (CH_3). The thermal displacement parameters for aromatic, CH and CH_2 groups were set as U_{iso}(H) = 1.2 U_{eq}(C) and for CH_3 groups as U_{iso}(H) = 1.5 U_{eq}(C). To identify hydrogen bonding within the crystal packing, the PARST software [23], integrated within the PLATON software package [24], was employed. Experimental parameters related to the X-ray analysis of the EAMTPQ are summarized in Table 1.

Table 1. *Experimental data for crystal structure determination of EAMTPQ*

CCDC deposition number	2281158	F_{000}	310
Empirical formula	$C_{36}H_{50}N_4O_2$	***Diffractometer***	STOE IPDS II
Color / shape	Yellow / plate	***Absorption correction***	Integration (X-RED32; Stoe & Cie, 2002)
Formula weight	570.80	T_{min}, T_{max}	0.9825, 0.9968
Radiation type, Wavelength (Å)	MoK_α, λ= 0.71073	***Θ range for data collection (°)***	$2.19 \leq \theta \leq 30.62$
Temperature (K)	293 (2)	***Index ranges***	$-8 \leq h \leq 7$, $-11 \leq k \leq 11$, $-16 \leq l \leq 15$
Crystal system	Triclinic	***Number of parameter***	195
Space group	$P\bar{1}$	***Reflections collected***	6222
Crystal size (mm)	0.51 × 0.26 × 0.07	***Independent / observed reflections***	3027 / 1201
Unit cell parameters			
a, b, c (Å)	6.8512 (9), 9.9748 (14), 13.892 (3)	***No. of restraints***	62
α, β, γ (°)	74.679 (13), 86.608 (13), 75.049 (11)	R_{int}	0.117
Volume (Å³)	884.6 (2)	$R[F^2 > 2\sigma(F^2)]$, $wR(F^2)$, S	0.098, 0.293, 0.92
Z	1	***R indices (all data)***	R_1= 0.1868, wR_2= 0.2361
Density (Mg/m³)	1.071	$\Delta\rho_{max}$, $\Delta\rho_{min}$, ($eÅ^{-3}$)	0.41, -0.19
μ (m/m¹)	0.067		

Computational Details

EAMTPQ was optimized and quantified using Gaussian03W software [25], and the results were visualized using GaussView 4.1.2 software [26]. In the optimization calculations, the B3LYP functional, comprising Becke's three-parameter exchange functional (B3) [27] and the Lee-Yang-Parr correlation functional (LYP) [28], was used in conjunction with the 6-31G(d,p) and 6-311G(d,p) basis sets. The compound's optimized geometry was utilized to calculate geometric parameters, which were then compared to experimental data. All theoretical calculations, except for HF analysis and MD, were performed using the DFT-B3LYP method with 6-31G(d,p) and 6-311G(d,p) basis sets. HOMO and LUMO energies were also computed. To evaluate the chemical reactivity of the molecule, the MEP surface map was analyzed with theoretical calculations at the B3LYP/6-31G(d,p) and B3LYP/6-311G(d,p) levels. The MEP map, electrostatic potential contour map, and FMOs were visualized with GaussView 4.1.2 software [26]. Hirshfeld surface (HS) analysis [29, 30], two-dimensional (2D) fingerprint plots [31], and interaction energy calculations were produced using Crystal Explorer Version 17.5 software, from the crystallographic information file [29]. The DFT-B3LYP method with the 6-311G(d,p) basis set was used for the input file of MD calculations. The current and fast online program, the Swiss ADME program [32, 33], was used to obtain information about some important criteria such as absorption, metabolism, distribution and excretion for the biological use of the synthesized molecule. MD simulation of BRAF V600e mutant protein (PDB ID: 5CSW) [13] was carried out with the

EAMTPQ compound, and Autodock Vina 1.5.6 simulation software [14] was used for the simulation. Biovia Discovery Studio software [15] was used for data visualization.

Results and Discussion

Structural Commentary

Half of the molecule is present in EAMTPQ's asymmetric unit, with the remaining part created by an inversion center situated at the midpoint of the C1-C1^{i} bond (Figure 2; symmetry code: (*i*) *-x, -y, -z+1*). In the asymmetric unit, the molecule consists of 2,2,8,8-tetramethyloctahydro-1*H*-quinolizine group, phenol ring and (*E*)-*N*-ethylidenemethanamine. The dihedral angles formed by the LSQ-planes between the C3-C8 ring and the C5/C6/N2/C14-C16 and C6/C7/C9-C11/N2 rings in the 2,2,8,8-tetramethyloctahydro-1*H*-quinolizine group are; 6.57(11)°, 6.78(14)° and 8.06(14)°, respectivelly. It is observed that the other five atoms exhibit an envelope conformation. Specifically, the C6 atom in the C3-C8 ring deviates from the mean plane by -0.0258(42), the C15 atom in the C5/C6/N2/C14-C16 ring, part of the 2,2,8,8-tetramethyloctahydro-1*H*-quinolizine group, deviates by 0.4016(77), and the C11 atom in the C6/C7/C9-C11/N2 ring deviates by -0.3926(56). Table 2 displays a selection of bond lengths and angles (bond and torsion), while the molecular structure is illustrated in Figure 2.

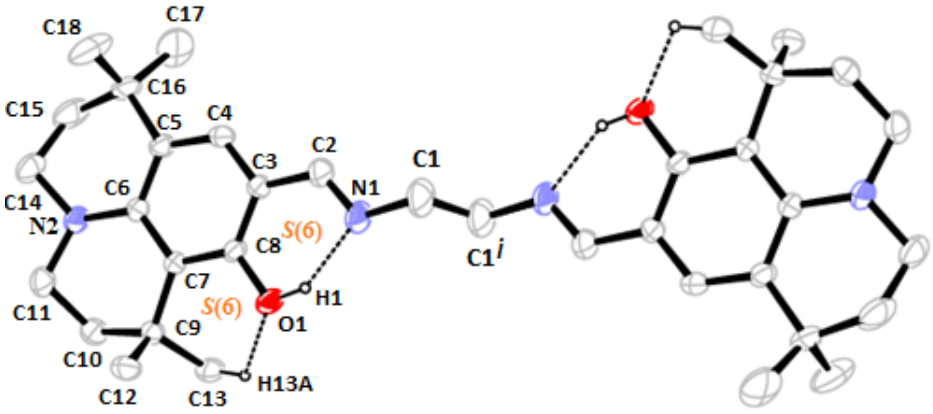

Figure 2. *The ORTEP-III diagram of EAMTPQ's, including the atom numbering scheme and intramolecular contacts. With a probability level of 20%, the displacement ellipsoids are depicted. [Symmetry code: (i) -x, -y, -z+1]*

As seen in Table 2, the lengths of the N1=C2, C2-C3 and C8-O1 bonds show that the compound prefers the OH tautomeric form over NH in the solid state. The bond lengths reported for similar OH-form compounds in the existing literature can be compared in a positive manner [34-38]. In the 2,2,8,8-tetramethyloctahydro-1*H*-quinolizine group, the C6-N2 and C14-N2 bond lengths in the C5/C6/N2/C14-C16 ring (Table 2) are consistent with those reported for similar structures [39,40]. Notably, the C14-C15, C15-C16, and C16-C5 bond lengths [1.533(8), 1.580(8), and 1.542(5) Å, respectively] display characteristics of a delocalized pyridine ring.

Table 2. *Some chosen parameters for EAMTPQ*

Geometric Parameters	Experimental [X-ray]	Calculated [DFT-B3LYP]	
		6-31G(d,p)	6-311G(d,p)
Bond Lengths (Å)			
O1-C8	1.362(4)	1.357	1.357
N1-C1	1.513(6)	1.490	1.492
N1-C2	1.275(6)	1.281	1.280
N2-C11	1.485(6)	1.475	1.481
N2-C14	1.461(5)	1.455	1.455
N2-C6	1.444(5)	1.391	1.398
Bond Angles (º)			
C1-N1-C2	120.0(5)	119.462	119.478
C6-N2-C14	121.3(4)	119.660	119.812
C11-N2-C14	110.6(4)	115.389	115.354
C6-N2-C11	120.2(3)	118.644	118.829
N1-C1-C1^{i}	116.1(7)	114.644	114.680
N1-C2-C3	124.0(5)	123.109	123.466
N2-C6-C7	120.3(3)	119.873	119.883
N2-C6-C5	120.7(3)	119.277	119.382
O1-C8-C3	117.4(3)	119.125	119.091
O1-C8-C7	119.5(3)	119.592	119.504
N2-C11-C10	104.6(4)	106.343	105.299
N2-C14-C15	104.0(4)	106.343	105.362
Torsion Angles (º)			
C8-C7-C6-N2	174.6(4)	174.730	174.643
C6-N2-C11-C10	49.1(6)	48.780	48.780
C9-C7-C8-O1	4.0(6)	3.353	3.639
O1-C8-C3-C4	178.5(4)	179.622	179.565
O1-C8-C3-C2	1.2(7)	0.610	0.763
C1-N1-C2-C3	178.4(5)	179.538	179.542
C2-N1-C1-C1^{i}	117.1(9)	119.882	119.580
N2-C14-C15-C16	61.9(6)	60.388	61.031
N2-C6-C5-C16	5.2(7)	2.224	2.247

Symmetry code: (*i*) *-x, -y, -z*+1.

EAMTPQ's crystal structure is stabilized by the strong intramolecular O1–H1···N1 and weak intramolecular C13–H13A···O1 hydrogen bonds (Figure 3), as well as the weak intermolecular C17–H17B···O1 and C1–H1A···*Cg*(1) interactions.

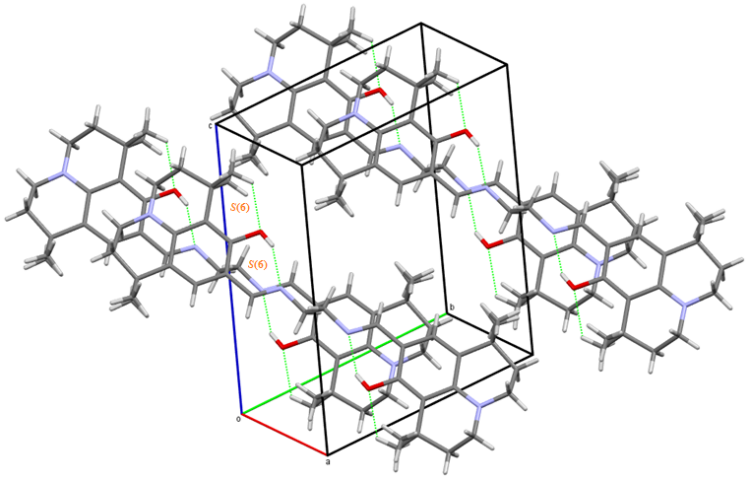

Figure 3. *The arrangement of intermolecular hydrogen bonds in EAMTPQ is illustrated, with hydrogen bonds represented as dashed green lines*

Intramolecular hydrogen bonds of the O–H···N and C–H···O types stabilize the molecular configuration of EAMTPQ, as demonstrated in Figure 3 and outlined in Table 3. In addition to these hydrogen bonds, we have noticed a C–H···π interaction, where the C1 and H1A atoms of the molecule, located at the asymmetric site, participate in a C1–H1A···π interaction with a phenol ring from a neighboring molecule at *1-x,-y,1-z*. The H1A···π distance in this interaction is 3.865(8) Å. This interaction links the molecules along the *b*-crystallographic axis, as illustrated in Figure 4 and specified in Table 3.

Table 3. *Geometry of hydrogen bonds in EAMTPQ*

D–H···A	**D–H [Å]**	**H···A [Å]**	**D···A [Å]**	**D–H···A [º]**
O1–H1···N1	0.82	1.92	2.661(5)	150.0
C13–H13A···O1	0.96	2.28	2.912(7)	123.0
C17–H17B···O1^{ii}	0.96	3.71	2.771(4)	165.1
D–H···*Cg*	**D–H [Å]**	**H···*Cg* [Å]**	**D···*Cg* [Å]**	**D–H···*Cg* [º]**
C1–H1A·· *Cg*(1)^{iii}	0.97	2.9419	3.865(8)	159.40

Symmetry code: [(ii) x, y+1, z; (iii) 1-x, -y, 1-z]. Cg(1) represents the centroid of the C3-C8 ring

The molecular configuration of EAMTPQ was also determined through theoretical calculations. DFT calculations were started by optimizing the molecule with X-ray diffraction coordinates, which were used to compare with experimental results and investigate electronic structures. Table 2 presents the theoretically derived molecular geometry for EAMTPQ. The X-ray structure was utilized as a starting point for optimizing the ground state with the 6-31G(d,p) and 6-311G(d,p) basis sets.

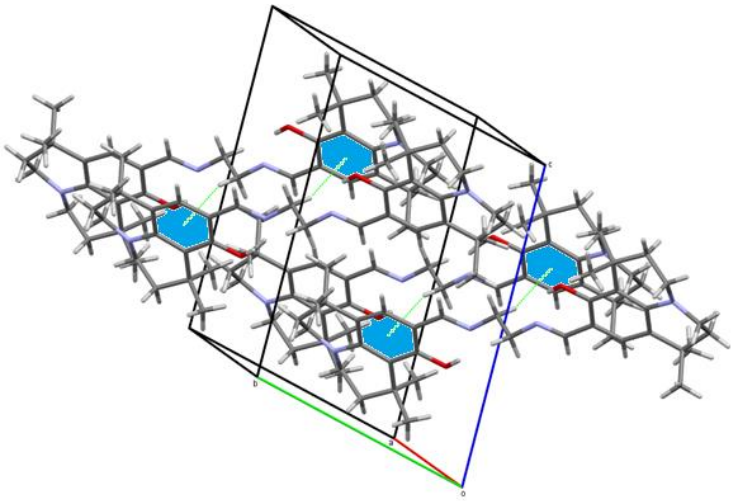

Figure 4. *C1–H1A···Cg(1) interactions in the EAMTPQ (interactions are shown in green dashed). Symmetry code: (iii) 1-x, -y, 1-z. Cg(1) represents the centroid of the C3-C8 ring*

In general, two primary methods were employed to examine the molecular structures. The initial technique was designed to calculate the correlation coefficient (R^2). The B3LYP/6-31G(d,p) and B3LYP/6-311G(d,p) methods were used to calculate optimized geometric parameters, including bond lengths, bond angles, and torsion angles. The results are summarized in Table 2. The regression equations for experimental and theoretical bond lengths and angles (bond and torsion) using the 6-31G(d,p) basis set were found to be $y = 0.1502 + 0.88382\ x$, $y = 25.933323 + 0.77948\ x$, and $y = -1.40243 + 1.01716\ x$, respectively. Similarly, for the 6-311G(d,p) basis set, the corresponding equations were $y = 0.12214 + 0.90517\ x$, $y = 18.70998 + 0.84051\ x$, and $y = -1.19641 + 1.01565\ x$, respectively. The calculated R^2 values for bond lengths were determined to be 0.97468 and 0.98025, for bond angles 0.96583 and 0.96638, and for torsion angles 0.99987 and 0.99989 at the B3LYP/6-31G(d,p) and B3LYP/6-311G(d,p) levels, respectively. Based on these correlation values, the B3LYP/6-311G(d,p) method demonstrated greater accuracy in predicting bond lengths and angles (bond and torsion) compared to the B3LYP/6-31G(d,p) method. The second approach for structural comparison involved overlaying the theoretical molecular framework with the experimental structure obtained through X-ray diffraction. This analysis yielded root-mean-square errors (RMSE) of 0.256 Å and 0.251 Å for the B3LYP/6-31G(d,p) and B3LYP/6-311G(d,p) levels, respectively (Figure 5). These findings suggest that the B3LYP/6-311G(d,p) method effectively replicates the molecular geometry of EAMTPQ. However, it is essential to emphasize that these theoretical computations were conducted under gas-phase conditions.

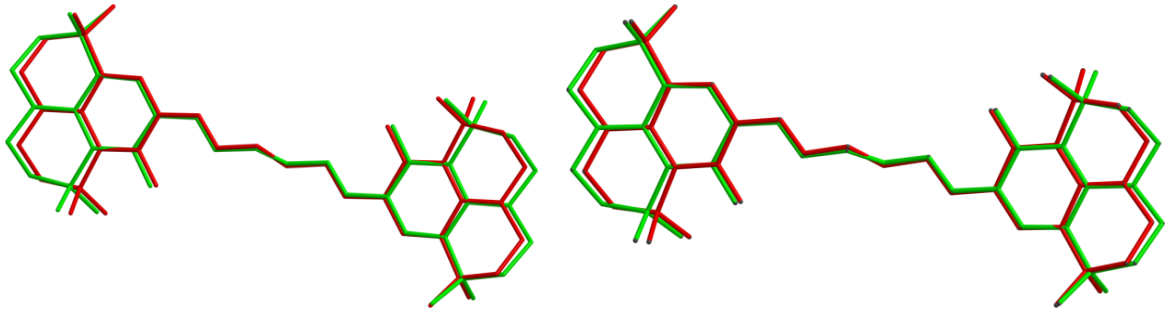

(a) **(b)**

Figure 5. *Superimposition of the calculated structures [(a) B3LYP/6-31G(d,p) (red), (b) B3LYP/6-311G(d,p) (red)] onto the X-ray structure (green) for EAMTPQ was done atom-by-atom. For clarity, hydrogen atoms are omitted*

FMOs

Quantum chemical parameters, which provide insight into a compound's chemical reactivity and kinetic stability, are fundamentally determined by FMOs. The HOMO and LUMO orbital distributions for the EAMTPQ molecule were computed at the B3LYP/6-31G (d, p) and B3LYP/6-311G (d, p) levels, with the results depicted in Figure 6.

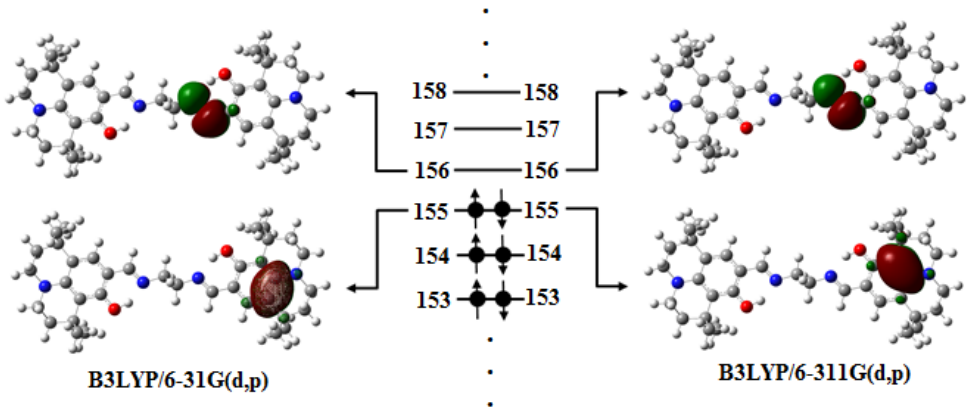

Figure 6. *The 3D plot of HOMO and LUMO orbitals of EAMTPQ*

Using the energy values of the HOMO and LUMO orbitals, key chemical properties can be determined through the following equations:

Electronegativity (χ) = (I + A) / 2

Chemical hardness (η) = (I - A) / 2

Chemical softness (S) = 1 / 2 η

Here, I and A correspond to the ionization potential and electron affinity respectively, which are derived from:

Ionization potential (I) = $-E_{HOMO}$

Electron affinity (A) = $-E_{LUMO}$

[41]. The calculated values for HOMO and LUMO energies, energy gap (ΔE), I, A, χ, η, and S were determined for the molecule at both computational levels and are presented in Table 4. The analysis

indicates that EAMTPQ consists of 155 occupied molecular orbitals. The energy values for HOMO and LUMO were identified as -4.9166 eV and -0.8865 eV, respectively, for the B3LYP/6-31G(d,p) level, while these values were -5.1329 eV and -1.0969 eV, respectively, for the B3LYP/6-311G(d,p) level. A significant HOMO-LUMO energy gap, calculated as 4.0301 eV for B3LYP/6-31G(d,p) and 4.0360 eV for B3LYP/6-311G(d,p), suggests low molecular polarity and reduced chemical reactivity, as outlined in Table 4.

Table 4. *Calculated boundary orbital energies, I, A, χ, η and S of the EAMTPQ*

Parameter	**B3LYP/6-31G (d, p)**	**B3LYP/6-311G (d, p)**
Total energy (a.u.)	-1771.52225323	-1771.89257551
E_{HOMO} (eV)	-4.9166	-5.1329
E_{LUMO} (eV)	-0.8865	-1.0969
ΔE (eV)	4.0301	4.0360
I (eV)	4.9166	5.1329
A (eV)	0.8865	1.0969
χ **(**eV)	2.9016	3.1149
η **(**eV)	2.0151	2.0180
S **(**1/eV**)**	0.2481	0.2478
μ (D)	1.3292	1.4281

MEP

The MEP provides insight into the electron density distribution within a molecule, highlighting regions that are likely to participate in electrophilic and nucleophilic interactions, as well as hydrogen bonding [42]. A color gradient is used to visualize these charge distributions: Red indicates electron-rich regions with partial negative charge, blue stands for electron-poor regions with partial positive charge, and yellow/light blue indicates regions with medium electron richness or electron deficiency. The potential scale spans from red (indicating the lowest potential) to blue (representing the highest potential) [43]. The MEP of EAMTPQ was computed using the DFT/B3LYP/6-31G(d,p) and DFT/B3LYP/6-311G(d,p) methods, and the corresponding results are depicted in Figure 7. The color scale for these calculations ranges from -0.0369 a.u. (red) to 0.0369 a.u. (blue) at the B3LYP/6-31G(d,p) level, and from -0.0359 a.u. (red) to 0.0359 a.u. (blue) at the B3LYP/6-311G(d,p) level. Notably, the most negative potential (red regions) is concentrated around the O1 and N1 atoms. As illustrated in Figure 7, electronegative atoms such as O1 and N1 are enveloped by red and yellow zones, signifying electron-rich sites that could serve as potential centers for electrophilic attack by positively charged species. Conversely, hydrogen atoms are encircled by blue regions, suggesting their suitability as sites for nucleophilic interactions. These areas are predicted to function as hydrogen bond acceptors. Furthermore, Figure 7 supports the existence of both intramolecular and intermolecular hydrogen bonding, as outlined in Table 3. Furthermore, a 2D representation of the MEP contour and total electron density is provided in Figure

7.c.1-2, illustrating that electron density values remain confined within a specific range along the (0010) plane.

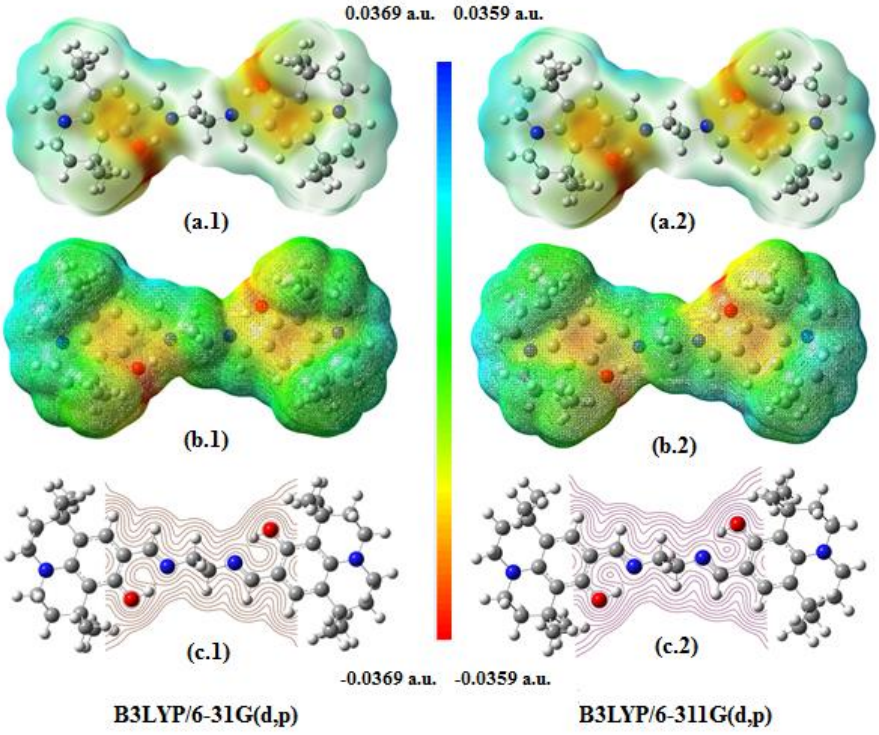

Figure 7. *(a) MEP) map, (b) MESH and (c) MEP contour total density* ***i****n gas phase of compound*

HS Analysis

In a recent study by Tiekink and coworkers [44], the use of HS analysis [31] and the related 2D fingerprint plots [30] for analyzing and quantifying intermolecular contacts in crystals were reviewed and highlighted. We also conducted similar calculations (mapping the surface over normalized contact distance (d_{norm}) and generating 2D fingerprint plots) using CrystalExplorer [45]. To comprehensively represent the interactions within the molecular crystal, we considered the entire molecule for the HS calculation. The primary objective was to provide an in-depth representation of the molecular interactions. The HS of the compound was modified to be represented by calculating the d_{norm}, and the resulting surface was visualized using colors like red, white, and blue. In the d_{norm} surface, blue regions represent positive electrostatic potentials, while red regions represent negative electrostatic potentials. The weak intermolecular interaction [(C17–H17B···O1^{ii}), symmetry code: (*ii*) *x*, *y+1*, *z*] is shown in Figure 8.

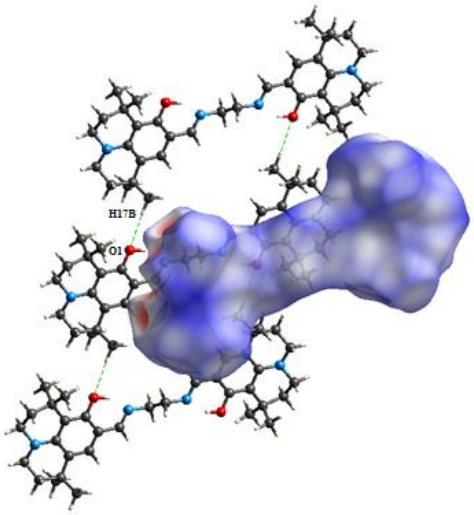

Figure 8. *HS represented by dnorm were used to illustrate the intermolecular interactions of the EAMTPQ compound*

The results revealed a range of intermolecular interactions in molecular crystals, with atomic sizes varying from -1.2398 (indicated by red) to 1.9070 (indicated by blue). The HS of the EAMTPQ, mapped over d_{norm}, is shown in Figure 9. The analysis of the HS of the compound incorporated several indicators, including d_i, d_e, shape index, curvedness, and fragment patches (Figure 9). Notably, d_i ranged from 0.7090 to 2.9473 Å, while d_e ranged from 0.3740 to 2.4867 Å. The observation at $d_i < d_e$ indicates a higher electron density at the HS of the crystal. Additionally, the shape index ranged from -0.998 to 0.996 in terms of atomic dimensions. The curvedness values varied from -4.067 to 0.717, where a high negative value indicates significant concavity and non-convexity on the HS, while a positive value suggests a moderately convex region, meaning the surface slightly protrudes outward. The fragment patch showed values between 0.0000 and 18.0000.

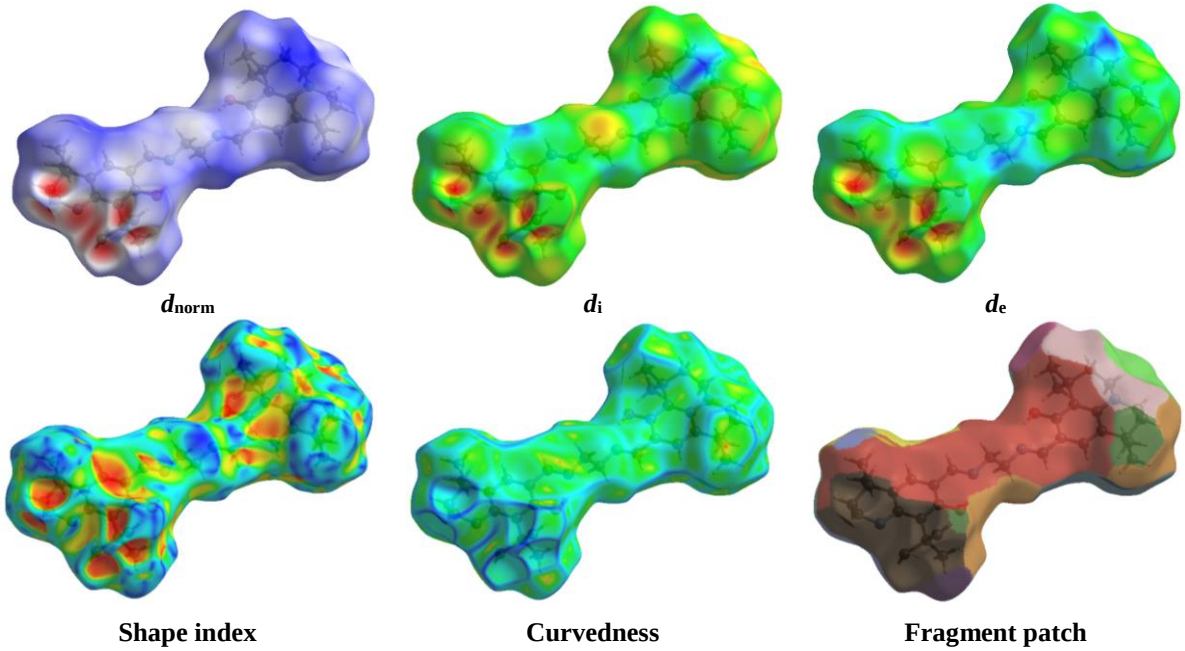

Figure 9. *Key parameters of the HSs: d_{norm}, d_i, d_e, shape index, curvedness, and fragment patch*

A 2D fingerprint map represents the angle between two vectors (d_i and d_e) representing the directions of interatomic contacts in two dimensions during the calculation of d_i and d_e. The d_{norm} value quantifies the distance from a point on the HS to the closest atomic center, adjusted by the total of the van der Waals radii of the adjacent atoms. In this context, d_e denotes the distance to the nearest atom outside the HS, while d_i denotes the distance to the nearest atom inside the surface [46]. The 2D fingerprint plots, showing the various interactions, are presented in Figure 10.a for all contacts. H···H intermolecular interactions are predominant, followed by C···H/H···C and O···H/H···O interactions that correspond to various types of C–H···π and C–H···O bonds. This is reflected in the contributions from H···H contacts at 77.7% (Figure 10.b), H···C/C···H contacts at 16.4% (Figure 10.c), and O···H/H···O at 2.7% (Figure 10.d). Minor contributions come from other contacts, such as N···H/H···N at 1.3% (Figure 10.e), N···C/C···N at 1.3% (Figure 10.f), C···C at 0.4% (Figure 10.g), and N···N contacts at 0.2% (Figure 10.h).

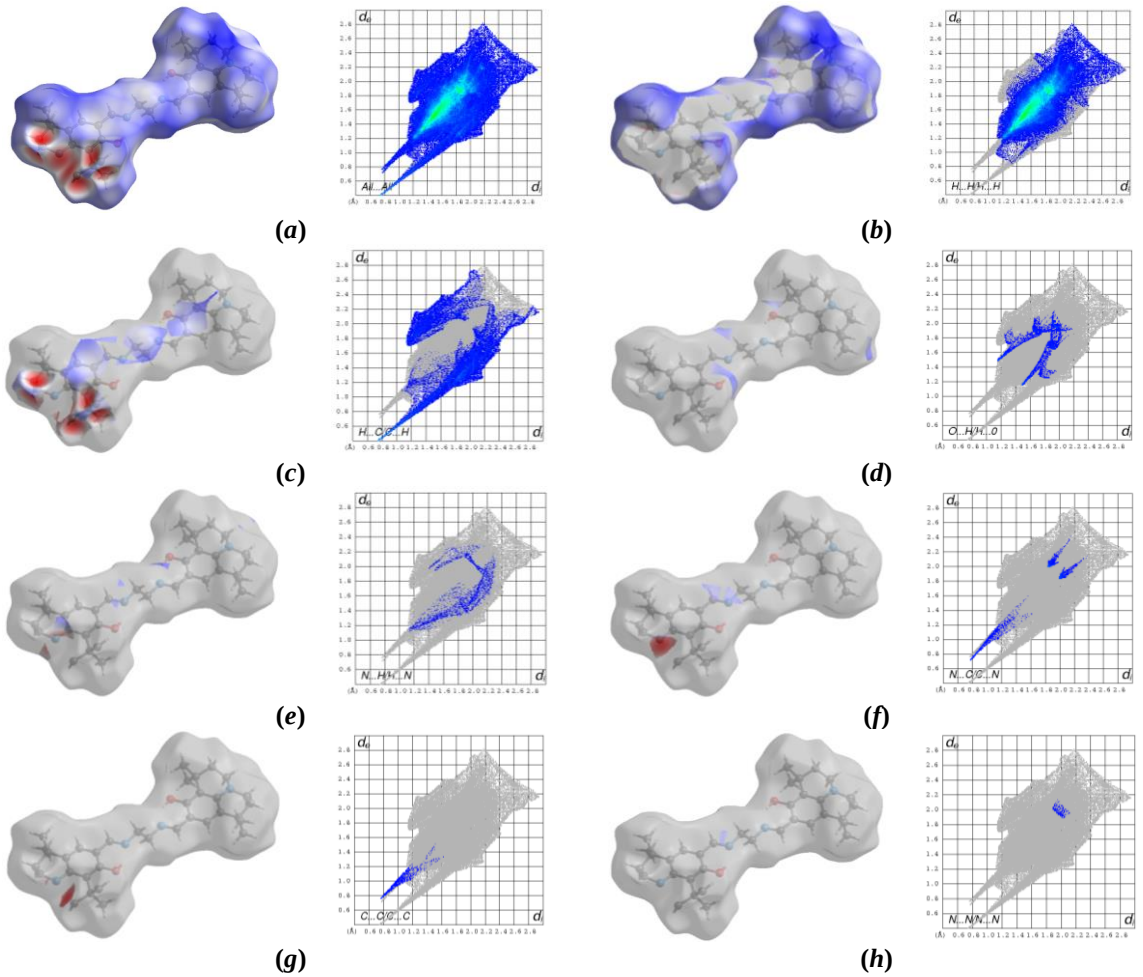

Figure 10. *(a) The complete 2D fingerprint plot for EAMTPQ, along with fingerprint plots separated into (b) H···H, (c) H···C/C···H, (d) O···H/H···O, (e) N···H/H···N, (f) N···C/C···N, (g) C···C, and (h) N···N contacts*

Drug-likeness

Lipophilicity, solubility, and flexibility are important criteria for drug design, and computational analysis is an effective way to investigate whether a compound is appropriate. For this purpose, an up-to-date and fast online program, the Swiss ADME program, was used [32, 33]. The program provides details on several key criteria for biologically utilized molecules, including absorption, distribution, metabolism, and excretion. The synthesized compound's properties have been calculated and are listed in Table 5.

Table 5. *In silico results of the EAMTPQ*

Physicochemical Properties

Formula	$C_{36}H_{50}N_4O_2$	**Num. H-bond accep.**	4
Molecular weight (g/mol)	570.81	**Fraction Csp³**	0.61
Num. heavy atoms	42	**TPSA (Å²).**	71.66
Num. rotatable bonds	5	**Num. H-bond donor**	2
Num. arom. heavy atoms	12	**Molar Refr.**	184.64

Lipophilicity		**Pharmacokinetics**			
Log $P_{o/w}$ (iLOGP)	5.61	**GI absorption**	High	**CYP2D6 inhibitor**	No
Log $P_{o/w}$ (XLOGP3)	7.37	**BBB permeant**	No	**CYP3A4 inhibitor**	No
Log $P_{o/w}$ (WLOGP)	6.21	**P-gp substrate**	Yes	**Log Kp (skin permeation)**	-4.55 cm/s
Log $P_{o/w}$ (MLOGP)	4.18	**CYP1A2 inhibitor**	No		
Log $P_{o/w}$ (SILICOS-IT)	8.57	**CYP2C19 inhibitor**	No	**CYP2C9 inhibitor**	No
Consensus Log $P_{o/w}$	6.39				

Water Solubility

	(ESOL)	**(Ali)**	**(SILICOS-IT)**
Log S	-7.90	-8.70	-9.54
Solubility	7.13e-06 mg/ml; 1.25e-08 mol/l	1.13e-06 mg/ml; 1.98e-09 mol/l	1.64e-07 mg/ml; 2.87e-10 mol/l
Class	Poorly soluble	Poorly soluble	Poorly soluble

Druglikeness	**Medicinal Chemistry**
Lipinski; No; 2 violations: MW>500, MLOGP>4.15	**PAINS; 0 alert**
Ghose; No; 4 violations: MW>480, WLOGP>5.6, MR>130, #atoms>70	**Leadlikeness;** No; 2 violations: MW>350, XLOGP3>3.5
Veber; Yes	**Brenk;** 1 alert: imine_1
Egan; No; 1 violation: WLOGP>5.88	**Synthetic accessibility;** 4.75
Muegge; No; 1 violation: XLOGP3>5	
Bioavailability Score; 0.17	

To evaluate the potential of the synthesized compound as a drug precursor, this study examined its compatibility based on various theoretical information. In this respect, the physicochemical properties such as molecular weight and saturated carbon number were first evaluated. When reviewing the bioavailability radar in Figure 11, the molecule demonstrates appropriate flexibility and unsaturation.

The synthesized molecule features a large, symmetrical structure, and consequently, its solubility and lipophilicity are within applicable ranges. The topological surface area and rotatable bond number are in an acceptable range. Conversely, H bond acceptor and donor activity are attractive properties for biological applications. As a result, the synthesized molecule raises concerns due to its large molecular structure regarding the Lipinski and Ghose rules, which are important indicators in drug design and application. When its medical properties are evaluated, it is promising that the molecule can be easily obtained. Another crucial criterion for the synthesized molecule is that it demonstrates high gastrointestinal absorption and is active as a P-gp substrate, as illustrated in the BOILED- egg graph in Figure 11.

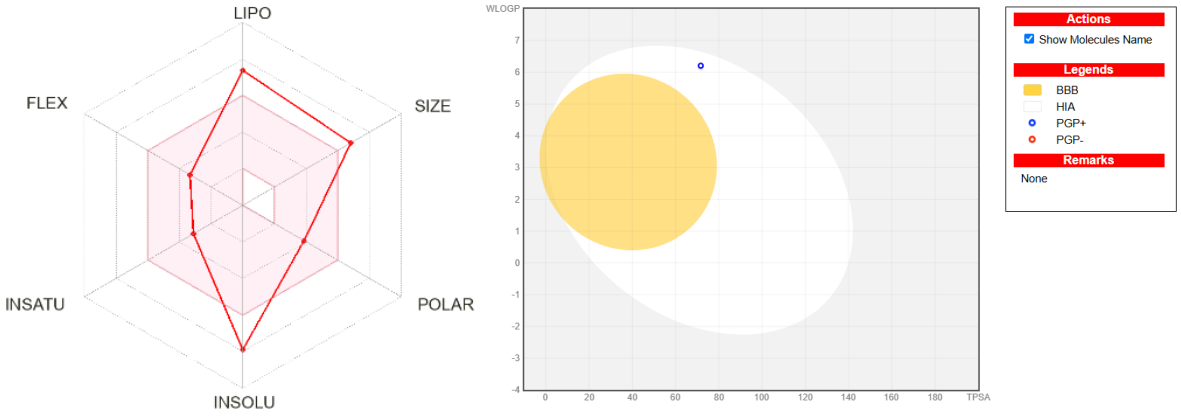

Figure 11. *Bioavailability radar and the BOILED-egg graph of the EAMTPQ*

MD Method

The MD is a method that simulates the binding of micro-scale ligand structures and macro-scale protein structures from suitable binding sites with a simulation program. The MD method has recently revealed its importance in this field with the increasing number of studies in the literature [47]. In particular, the increasing importance of computer-aided drug design and technological developments have increased the need for simulation programs in this field. This method enables the determination of the specific binding site of a protein and the visualization of the binding geometry of the ligand suitable for this site, thus enabling appropriate protein-ligand interactions to be realized. This method also enables the discovery of new protein and ligand structures by taking proteins and ligands with known structures as references [48]. The MD method is frequently preferred for the determination of suitable small molecule ligands, especially for the treatment of diseases arising from anomalies in the structure of proteins and genes.

Protein and Ligand Protein Preperation for MD Simulation

The first step to perform a MD simulation is to determine and prepare the appropriate protein structure. Different databases can be used to obtain the protein structure. Some of these databases are listed as the protein data bank [49], uniprot [50] and alphafold protein structure database [51]. When the protein

structure is obtained from any database, the protein preparation phase can be started. For this preparation phase, first of all, water molecules on the surface of the protein structure, if any, are removed and then hydrogens are added to the structure. Thus, the protein structure is basically prepared. Ligand preparation is started by selecting the rotating bonds in the structure of the molecule. After the selection of the appropriate bonds, the ligand is ready for binding. The binding simulation can be started by selecting the appropriate algorithms for the calculation.

MD Studies

The MD simulation data of EAMTPQ and BRAF V600E mutant protein are presented in Table 6.

Table 6. *Simulation data of EAMTPQ compound and BRAF V600E mutant protein*

Molecule	Binding Affinity (kcal/mol)	H-bond Interaction
EAMTPQ	-9.4	LEU258
		SER344
		SER341

Visualization of simulation data of EAMTPQ compound and BRAF V600E mutant protein is presented in Figure 12.

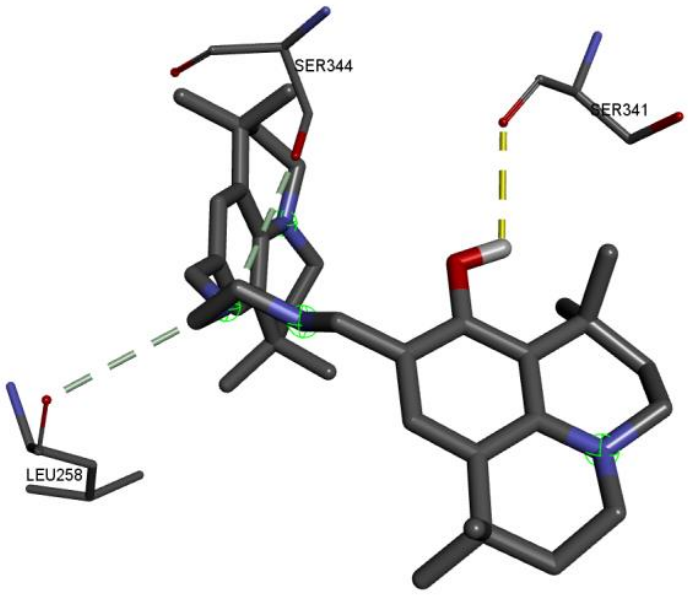

Figure 12. *Molecular geometry of the interaction between EAMTPQ and BRAF V600E mutant protein*

When Table 6 is examined, the value of the binding affinity between the protein and the ligand is calculated as -9.4 kcal/mol. This value enables us to conclude that the interaction between the macro-sized protein and the micro-sized ligand is strong. When both the table and Figure 12 are examined, it is observed that the hydrogen bond, which is a parameter that allows us to comment on the strength of

the interaction observed in protein-ligand interactions, is established between the EAMTPQ molecule and the amino acids LEU258, SER341 and SER344. Thus, the hydrogen bond present in the interaction allows the detection of special binding sites in the structure of the protein and the directionality of the interaction [52].

Conclusion

In conclusion, the EAMTPQ molecule was synthesized and characterized through X-ray crystallography. The electronic properties and geometric parameters were explored using DFT calculations (B3LYP/6-31G(d,p) and B3LYP/6-311G(d,p) levels). While the computational results showed slight discrepancies from the experimental data, these differences can be attributed to the fact that the compound was considered in the gas phase in the computational model. Theoretical results also provided insights into the FMOs and related parameters. The MEP maps revealed the critical role of active sites in chemical bonding, aiding in the synthesis of new compounds. The maps showed regions of negative potential on electronegative atoms and regions of positive potential around hydrogen atoms, confirming the presence of hydrogen bonds in the crystal structure. HS analysis showed that the primary interactions contributing to the crystal packing were H···H (77.7%) and H···C/C···H (16.4%) interactions. The protein-ligand binding affinity was calculated to be -9.4 kcal/mol, showing a strong interaction between the macromolecule and the small ligand. Hydrogen bonds between the EAMTPQ molecule and the amino acids LEU258, SER341, and SER344 were identified, shedding light on specific binding sites in the protein structure and the directionality of the interaction.

Acknowledgements This study was supported by Sinop University Scientific Research Coordination Unit. Project Number: BMYO-1901-21—001, 2023.

Funding/Financial Disclosure The authors received no financial support for the research, writing or publication of this study.

Ethics Committee Approval and Permissions The study does not require ethics committee permission or any special permission.

Conflict of Interests - All authors declare no conflict of interest that could effect the current study.

Authors Contribution Authors contributed equally to the study. All authors read and approved the final manuscript

References

[1] Katritzky, A. R., Rachwal, B., Rachwal, S., & Abboud, K. A. (1996). Convenient synthesis of julolidines using benzotriazole methodology. *The Journal of Organic Chemistry*, *61*(9), 3117-3126. https://doi.org/10.1021/jo9519118

[2] Martini, G., Martinelli, E., Ruggeri, G., Galli, G., & Pucci, A. (2015). Julolidine fluorescent molecular rotors as vapour sensing probes in polystyrene films. *Dyes Pigments*, *113*, 47-54. https://doi.org/10.1016/j.dyepig.2014.07.025

[3] Wu, W. H., Wang, Y., Zhou, Y. X., Shao, Y., Zhang, L. H., & Li, H. (2015). Selective fluorescence lighting-up recognition of DNA abasic site environment possessing guanine context. *Sensors and Actuators B: Chemical*, *206*, 449-455. http://dx.doi.org/10.1016/j.snb.2014.09.090

[4] Avhad, K., Jadhav, M., Patil, D., Chowdhury, T. H., Islam, A., Bedja, I., & Sekar, N. (2019). Rhodanine- 3-acetic acid containing D-π-A push-pull chromophores: effect of methoxy group on the performance of dye-sensitized solar cells. *Organic Electronics*, *65*, 386-393. https://doi.org/10.1016/j.orgel.2018.11.041

[5] Halter, O., & Plenio, H. (2018). Fluorescent dyes in organometallic chemistry: Coumarin-tagged NHC-metal complexes. *European Journal of Inorganic Chemistry*, *2018*(25), 2935-2943. https://doi.org/10.1002/ejic.201800395

[6] Lichlyter, D. J., & Haidekker, M. A. (2009). Immobilization techniques for molecular rotors-Towards a solid-state viscosity sensor platform. *Sensors and Actuators B: Chemical*, *139*(2), 648-656. https://doi.org/10.1016/j.snb.2009.03.073

[7] Royal, J. S., & Torkelson, J. M. (1992). Molecular-scale asymmetry and memory behavior in poly (vinyl acetate) monitored with mobility-sensitive fluorescent molecules. *Macromolecules*, *25*(6), 1705-1710.

[8] Boldt, P., Eisenträger, T., Glania, C., Göldenitz, J., Krämer, P., Matschiner, R., Rase, J., Schwesinger, R., Wichern, J., & Wortmann, R. (1996). Guanidyl and phosphoraniminyl substituents: New electron donors in second-order nonlinear optical chromophores. *Advanced Materials*, *8*(8), 672-675. https://doi.org/10.1002/adma.19960080817

[9] Chavan, N. D., & Vijayakumar, V., (2024). Synthesis, DFT studies on a series of tunable quinoline derivatives. *The Royal Society of Chemistry Advances*, *14*(29), 21089-21101. https://doi.org/10.1039/D4RA03961K

[10] Khalid, M., Akbar, A., Jawaria, R., Asghar, M. A., Asim, S., Khan, M. U., Hussain, R., Rehman, M. F., Ennis, C. J., & Akram, M. S. (2020). First principles study of electronic and nonlinear optical properties of A-D-π-A and D-A-D-π-a configured compounds containing novel quinoline-carbazole derivatives, *The Royal Society of Chemistry Advances*, *10*, 22273-22283. https://doi.org/10.1039/D0RA02857F

[11] Jamal, A., Ferjani, H., Faizi, M. S. H., Alzahrani, A. Y. A. (2024). DFT calculation and molecular docking studies of designing quinoline-derived anti-Alzheimer agents with NLO response. *Journal of the Indian Chemical Society*, *101*(8), 101181. https://doi.org/10.1016/j.jics.2024.101181

[12] Ahamed, A. A., Alharbi, S. A., & Venkatesan, G. (2024). A julolidine aldehyde dansyl hydrazine Schiff Base as fluorescence chemosensor for Zn^{2+} ions recognition and its application. *Journal of Fluorescence*, 1-11. https://doi.org/10.1007/s10895-024-03842-2

[13] Waizenegger, I. C., Baum, A., Steurer, S., Stadtmüller, H., Bader, G., Schaaf, O., Garin-Chesa, P., Schlattl, A., Schweifer, N., Haslinger, C., Colbatzky, F., Mousa, S., Kalkuhl, A., Kraut, N., & Adolf, G. R. (2016). A novel RAF kinase inhibitor with DFG-out-binding mode: High efficacy in BRAF-mutant tumor xenograft models in the absence of normal tissue hyperproliferation. *Molecular Cancer Therapeutics*, *15*(3), 354-365. https://doi.org/10.1158/1535-7163.MCT-15-0654

[14] Morris, G. M., Huey, R., Lindstrom, W., Sanner, M. F., Belew, R. K., Goodsell, D. S., & Olson, A. J. (2009). Autodock4 and AutoDockTools4: Automated docking with selective receptor flexibility. *Journal of Computational Chemistry*, *30*(16), 2785-2791. https://doi.org/10.1002/jcc.21256

[15] Kemmish, H., Fasnacht, M., & Yan, L. (2017). Fully automated antibody structure prediction using BIOVIA tools: Validation study. *PLoS One*, *12*(5), e0177923. https://doi.org/10.1371/journal.pone.0177923

[16] Meral, S., Agar, A. A. (2024). Synthesis, characterization and effects to cholesteric lyotropic liquid crystal media of -ONNO- type Schiff Bases and metal complexes. *Bulgarian Chemical Communations*, *56*(3), 274-281.

[17] Stoe, C. (2002). X-area (version 1.18) and Xred32 (version 1.04), Stoe & Cie, Darmstadt, Germany.

[18] Sheldrick, G. M. (2015). SHELXT-Integrated space-group and crystal-structure determination. *Acta Crystallographica Section A: Foundations and Advances*, *71*(1), 3-8. https://doi.org/10.1107/S2053273314026370

[19] Sheldrick, G. M. (2018). SHELXL-2018 Program for crystal structure refinement. University of Göttingen, Göttingen.

[20] Farrugia, L. J. (1999). WinGX suite for smallmolecule single-crystal crystallography. *Journal of Applied Crystallography*, *32*(4), 837-838. http://dx.doi.org/10.1107/S0021889899006020

[21] Farrugia, L. J. (1997). It ORTEP-3 for Windows-A version of it ORTEP-III with a graphical user interface (GUI). *Journal of Applied Crystallography*, *30*, 565. https://doi.org/10.1107/S0021889897003117

[22] Macrae, C. F., Edgington, P. R., McCabe, P., Pidcock, E., Shields, G. P., Taylor, R., Towler, M., & Streek, J. V. D. (2006). Mercury: Visualization and analysis of crystal structures. *Journal of Applied Crystallography*, *39*, 453-457. http://dx.doi.org/10.1107/S002188980600731X

[23] Nardelli, M. (1995). PARST95-An update to PARST: A system of Fortran routines for calculating molecular structure parameters from the results of crystal structure analyses. *Journal of Applied Crystallography*, *28*, 659. http://dx.doi.org/10.1107/S0021889895007138

[24] Spek, A. L. (2005). PLATON-a multipurpose crystallographic tool, Utrecht University, Utrecht.

[25] Frisch, M. J., Trucks, G. W., Schlegel, H. B., Scuseria, G. E., Robb, M. A., Cheeseman, J. R., Scalmani, G., Barone, V., Mennucci, B., Petersson, G. A., Nakatsuji, H., Caricato, M., Li, X., Hratchian, H. P., Izmaylov, A. F., Bloino, J., Zheng, G., Sonnenberg, J. L., Hada, M., Ehara, M., Toyota, K., Fukuda, R., Hasegawa, J., Ishida, M., Nakajima, T., Honda, Y., Kitao, O., Nakai, H., Vreven, T., Montgomery Jr., J. A., Peralta, J. E., Ogliaro, F., Bearpark, M., Heyd, J. J., Brothers, E., Kudin, K. N., Staroverov, V. N., Kobayashi, R., Normand, J., Raghavachari, K., Rendell, A., Burant, J. C., Iyengar, S. S., Tomasi, J., Cossi, M., Rega, N., Millam, J. M., Klene, M., Knox, J. E., Cross, J. B., Bakken, V., Adamo, C., Jaramillo, J., Gomperts, R., Stratmann, R. E., Yazyev, O., Austin, A. J., Cammi, R., Pomelli, C., Ochterski, J. W., Martin, R. L., Morokuma, K., Zakrzewski, V. G., Voth, G. A., Salvador, P., Dannenberg, J. J., Dapprich, S., Daniels, A. D., Farkas, O., Foresman, J. B., Ortiz, J. V., Cioslowski, J., & Fox, D. J. (2009). Gaussian 09, revision E.01, Gaussian, Inc., Wallingford CT.

[26] Dennington, R., Keith, T., & Millam, J. (2007) Gauss View, Version 4.1.2. Semichem Inc., Shawnee Mission.

[27] Becke, A. D. (1993). Density-functional thermochemistry. III. The role of exact exchange, *Journal of Chemical Physics*, *98*, 5648-5652. https://doi.org/10.1063/1.464913

[28] Lee, C, Yang, W, & Parr, R. G. (1998). Development of the Colle-Salvetti correlation-energy formula into a functional of the electron density, *Physical Review B*, *37*, 785-789. https://doi.org/10.1103/PhysRevB.37.785

[29] Turner, M. J., McKinnon, J. J., Wolff, S. K., Grimwood, D. J., Spackman, P. R., Jayatilaka, D., & Spackman, M. A. (2017). CrystalExplorer17, University of Western Australia, Perth.

[30] McKinnon, J. J., Jayatilaka, D., & Spackman, M. A. (2007). Towards quantitative analysis of intermolecular interactions with Hirshfeld surfaces. *Chemical Communications*, *37*, 3814-3816. http://dx.doi.org/10.1039/b704980c

[31] Spackman, M. A., & Jayatilaka, D. (2009). Hirshfeld surface analysis. *Crystal Engineering Communication*, *Royal Society of Chemistry*, *11*(1), 19-32. http://dx.doi.org/10.1039/B818330A

[32] Daina, A., Michielin, O., & Zoete, V. (2014). iLOGP: a simple, robust, and efficient description of n-octanol/water partition coefficient for drug design using the GB/SA approach, *Journal of Chemical Information and Modeling*, *54*(12), 3284-3301. https://doi.org/10.1021/ci500467k

[33] Daina, A., Michielin, O., & Zoete, V. (2017) SwissADME: A free web tool to evaluate pharmacokinetics, drug-likeness and medicinal chemistry friendliness of small molecules. *Scientific Reports*, *7*, 42717. https://doi.org/10.1038/srep42717

[34] Evecen, M., Ersanlı, C. C., Doğan, O. E., Bozkurt, İ., & Ağar, E. (2025). Synthesis and analysis thermodynamic electronic NLO, FMO, NBO, MEP, IR, UV, NMR properties Hirshfeld surface analysis and molecular docking of the new Schiff base molecule (*Z*)-4-bromo-2-(((2,4-dimethoxypheny)limino)methyl)-5-fluorophenol. *Journal of Molecular Structure*, *1329*, 1-14. https://doi.org/10.1016/j.molstruc.2025.141454

[35] Keleşoğlu, Z., Albayrak Kaştaş, Ç., Kaştaş, G., & Ersanlı, C. C. (2021). Synthesis, crystal structure, computational chemistry studies and Hirshfeld surface analysis of two Schiff Bases, (*E*)-2-[(4-bromo-2-methylphenylimino)methyl]-4-methylphenol and (*E*)-2-[(4-bromo-2-methylphenylimino) methyl]-6-methylphenol. *Molecular Crystals and Liquid Crystals*, *723*, 45-61. https://doi.org/10.1080/15421406.2020.1871178

[36] Koşar Kırca, B., Albayrak Kaştaş, Ç., & Ersanlı, C. C. (2021). Molecular and electronic structures of two new Schiff Base compounds (*E*)-2-Bromo-6-[(2-bromo-4-methylphenylimino) methyl]-4-chlorophenol and (*E*)-2-Bromo-6-[(4-bromo-3-methylphenylimino)methyl]-4-chlorophenol. *Journal of Molecular Structure*, *1241*(130643), 1-12. https://dx.doi.org/10.1016/j.molstruc.2021.130643

[37] Kaştaş, G., Albayrak Kaştaş, Ç., Ersanlı, C. C., & Koşar Kırca, B. (2020). Investigation of the molecular structure of (*E*)-2-Bromo-6-[(4-bromo-2-methylphenylimino)methyl]-4-chlorophenol. *Crystallography Reports*, *65*(3), 463-467. https://dx.doi.org/10.1134/S1063774520030153

[38] Kaştaş, G., Albayrak Kaştaş, Ç., Koşar Kırca, B., & Ersanlı, C. C. (2020). The effect of the change in substituents positions on the formation of supramolecular networks and the solvent type substituent dependence of prototropic behavior in three new *o*-hydroxy Schiff Bases. *Journal of Molecular Structure*, *1200*, 1-13. https://dx.doi.org/10.1016/j.molstruc.2019.127109

[39] İnaç, H. (2023). Crystal Structure of Zwitterionic (*E*)-9-(((3-hydroxyphenyl)iminio)methyl)-1,2,3,5,6,7-hexahydropyrido[3,2,1-ij]quinolin-8-olate. *International Scientific and Vocational Studies Journal*, *7*(2), 72-78. https://doi.org/10.47897/bilmes.1316337

[40] Kantar, E. N., Köysal, Y., Akdemir, N., Ağar, A. A., & Soylu, M. S. (2013). 8-{(*E*)-[(4-chloro-phen-yl)imino]-meth-yl}-1,1,7,7-tetra-methyl-1,2,3,5,6,7-hexa-hydro-pyrido[3,2,1-ij]quinolin-9-ol. *Acta Crystallographica Section E*, *69*(6), o883. https://doi.org/10.1107/S1600536813012579

[41] Pearson, R. G. (1986) Absolute electronegativity and hardness correlated with molecular orbital theory. *Proceedings of the National Academy of Sciences of the United States of America*, *83*, 8440-8441. http://dx.doi.org/10.1073/pnas.83.22.8440

[42] Guidara, S., Feki, H., & Abid, Y. (2015). Structural, vibrational, NLO, MEP, NBO analysis and DFT calculation of bis 2,5-dimethylanilinium sulfate. *Journal of Molecular Structure*, *1080*, 176-187. http://dx.doi.org/10.1016/j.molstruc.2014.09.084

[43] Saravanan, R., Seshadri, S., Günasekaran, S, Mendoza-Meroño, R., & García-Granda, S. (2015). Conformational analysis, x-ray crystallographic, FT-IR, FT-Raman, DFT, MEP and molecular docking studies on 1-(1-(3-methoxyphenyl) ethylidene) thiosemicarbazide. *Spectrochimica Acta - Part A: Molecular and Biomolecular Spectroscopy*, *139*, 321-328. http://dx.doi.org/doi:10.1016/j.saa.2014.12.026

[44] Tan, S. L., Jotani, M. M., & Tiekink, E. R. T. (2019). Utilizing Hirshfeld surface calculations, non-covalent inter-action (NCI) plots and the calculation of inter-action energies in the analysis of molecular packing. *Acta Crystallographica Section E*, *75*, 308-318. https://doi.org/10.1107/S2056989019001129

[45] Spackman, P. R., Turner, M. J., McKinnon, J. J., Wolff, S. K., Grimwood, D. J., Jayatilaka, D., & Spackman, M. A. (2021). CrystalExplorer: a program for Hirshfeld surface analysis, visualization and qu-antitative analysis of molecular crystals. *Journal of Applied Crystallography*, *54*(3), 1006-1011. https://doi.org/10.1107/S1600576721002910

[46] Abdel-Aal, S. K.; & Ouasri, A. (2022). Crystal structure, Hirshfeld surfaces and vibrational studies of tetrachlorocobaltate hybrid perovskite salts $NH_3(CH_2)_nNH_3CoCl_4$ (n=4, 9). *Journal of Molecular Structure*, *1251*, 131997. https://doi.org/10.1016/j.molstruc.2021.131997

[47] Başak, S. (2023). *Investigation of some schiff base molecules with antitumor and anticarsinogenic effects by molecular docking method*. (Tez no. 815683) [Master Thesis, Sinop University]

[48] Shoichet, B. K., Leach, A. R., & Kuntz, I. D. (1999). Ligand solvation in molecular docking. *Proteins*, *34*(1), 4-16. https://doi.org/10.1002/(sici)1097-0134(19990101)34:1<4::aid-prot2>3.0.co;2-6

[49] Berman, H. M., Westbrook, J., Feng, Z., Gilliland, G., Bhat, T. N., Weissig, H., & Bourne, P. E. (2000). The Protein Data Bank. *Nucleic Acids Research*, *28*(1), 235-242. https://doi.org/10.1093/nar/28.1.235

[50] The UniProt Consortium. (2023). UniProt: The Universal Protein Knowledgebase in 2023. *Nucleic Acids Research*, *51*(D1), D523-D531. https://doi.org/10.1093/nar/gkac1052

[51] Jumper, J., Evans, R., Pritzel, A., Green, T., Figurnov, M., Ronneberger, O., & Hassabis, D. (2021). Highly accurate protein structure prediction with AlphaFold. *Nature*, *596*(7873), 583-589. https://doi.org/10.1038/s41586-021-03819-2

[52] Başak, S., & Ersanlı, C. C. (2024). Investigation of Hirshfeld surface analysis and anticarcinogenic properties of Schiff Base containing compounds by molecular docking method. Hüsniye Sağlıker, (Ed), *Original Research and Reviews in Science and Mathematics*, (pp. 77-92).